Progress In Electromagnetics Research Letters, Vol. 47, 85–90, 2014

Ferrite-Loaded Half Mode Substrate Integrated Waveguide Phase Shifter

Yu Jian Cheng[1, *], Qiu Dong Huang[1], Ye Di Zhou[1], and Cheng Xiang Weng[2]

Abstract—An X-band ferrite-loaded half mode substrate integrated waveguide (HMSIW) phase shifter is proposed and fabricated in this paper. A full-height E-plane Yttrium Iron Garnet (YIG) ferrite slab is embedded in the HMSIW to construct the non-reciprocal phase shifter. With the application of a magnetic bias field on the ferrite slab, the phase of the ferrite-loaded HMSIW can be adjusted and controlled. For a magnetic bias field of 1800 Gauss, the insertion loss is less than 3.2 dB from 9.7 to 11.0 GHz. The return loss is better than 10 dB over the same frequency range. The largest differential phase shift can be up to 337°. This circuit is easily integrated with other planar components and also has the capability to handle medium power level.

1. INTRODUCTION

The currently popular substrate integrated waveguide (SIW) technique, also called as post-wall waveguide or laminated waveguide, combines the best and complementary features of both planar transmission lines and non-planar waveguides [1–4]. Thus it is found very appropriate in microwave and millimeter-wave applications, which have been validated by several successful designs. However, sometime the size of SIW blocks may be too large for practical circuits, and affect the integration. To overcome this drawback, an improved guided-wave structure, called half model substrate integrated waveguide (HMSIW) is proposed in [5–7].

In very recent years, researchers try to realize some SIW reconfigurable components by use of PIN diodes and varactors [8–15]. Unlike those conventional planar transmission lines, such as the microstrip line, the SIW is a uniconductor guided-wave structure and has the same electric potential for each metallic surface. Therefore, some difficulties exist in electronically tunable SIW designs. Besides, complex DC bias circuits may lead to unwanted leakage and interference.

Tuning operation characteristics of SIW components by magnetic field is another possible way. Some ferrite-loaded SIW components have been proposed [16–20], including isolators, switches, frequency-agile resonators, reconfigurable antennas, etc. Another important application of ferrite materials is in phase shifters, which are two-port components that provide variable phase shift by changing the bias field of the ferrite.

In this paper, we will concentrate on the design of an X-band HMSIW non-reciprocal phase shifter. A full-height E-plane ferrite slab is embedded in the HMSIW. With the application of a magnetic bias field on the ferrite slab, the propagation constant of the ferrite-loaded HMSIW is changed, thereby modifying the phase of the ferrite-loaded HMSIW.

Received 24 May 2014, Accepted 13 July 2014, Scheduled 30 July 2014

* Corresponding author: Yu Jian Cheng (chengyujian@uestc.edu.cn).

[1] Fundamental Science on Extreme High Frequency Laboratory, School of Electronic Engineering, University of Electronic Science and Technology of China, Chengdu 611731, P. R. China. [2] Electronic Countermeasure Laboratory, Air Force Early Warming Academy, Wuhan, P. R. China.

2. DESIGN PROCESS

2.1. Ferrite Material

As well known, ferrite materials have a significant amount of anisotropy at microwave frequency, which can be induced by applying a magnetic bias field. In this case, the magnetic dipoles in the ferrite material are forced to precess at a frequency controlled by the strength of the bias field [21]. A circularly polarized microwave signal in the same direction as this precession will interact strongly with the dipole moments. Therefore, the interaction with an applied microwave signal can be controlled by adjusting the strength of the bias field.

As one of the most commonly used ferrite materials, Yttrium Iron Garnet (YIG) ferrite is employed in this design. Its saturation magnetization value is 1850 Gauss, relative dielectric constant is 14.5, and 3 dB line width is 20 Oe. Figure 1 illustrates the calculated YIG effective relative permeability against the internal transverse magnetic fields H_0 for frequency 9, 9.5, 10, 10.5 and 11 GHz, respectively. The used equations can be found in [21]. As shown in Figure 1, the effective relative permeability of this material can be controlled by the magnetic bias field. Besides, such a ferrite material has the resonance permeability at a 1370 Gauss bias field for the frequency 9 GHz. At 11 GHz, such a magnetic field value is increased to 2080 Gauss.

2.2. Ferrite-Load Half Mode Substrate Integrated Waveguide

Figure 2 illustrates the geometry of a ferrite-loaded HMSIW section. A HMSIW is loaded with a vertical ferrite slab biased in the y direction. In this figure, a is the equivalent width of the HMSIW, w the slab width, c the slab offset, and h the substrate thickness. Here, the permeability tensor for z bias will be

$$[\mu] = \begin{bmatrix} \mu & j\kappa & 0 \\ -j\kappa & \mu & 0 \\ 0 & 0 & \mu_0 \end{bmatrix} \tag{1}$$

According to the Maxwell's equations in the ferrite slab region and dielectric region, as well as the HMSIW boundary conditions (PEC boundary: $z = 0$, h and $y = 0$; PMC boundary: $y = a$), the following transcendental equation can be given for calculation the propagation constant, β, in the ferrite-loaded HMSIW through a similar derivative process for a waveguide with E-plane full-height ferrite slab as described in [21].

$$\left(\frac{k_f}{\mu_e}\right)^2 + \left(\frac{\kappa\beta}{\mu\mu_e}\right)^2 - k_d \cot k_d c \left(\frac{k_f}{\mu_0\mu_e}\cot k_f w + \frac{\kappa\beta}{\mu_0\mu\mu_e}\right) - \left(\frac{k_d}{\mu_0}\right)^2$$
$$\times \cot k_d \cot k_d(2a - c - w) - k_d \cot k_d(2a - c - w)\left(\frac{k_f}{\mu_0\mu_e}\cot k_f w - \frac{\kappa\beta}{\mu_0\mu\mu_e}\right) = 0 \tag{2}$$

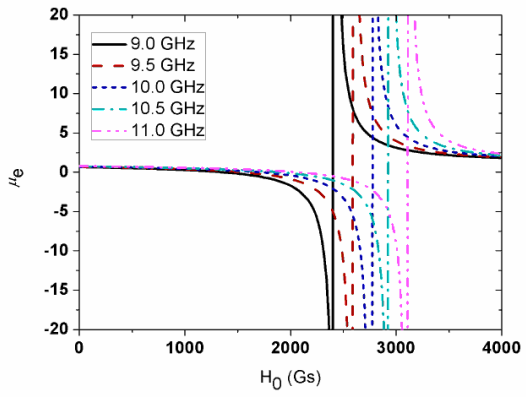

Figure 1. YIG effective relative permeability versus magnetic bias field at different frequencies.

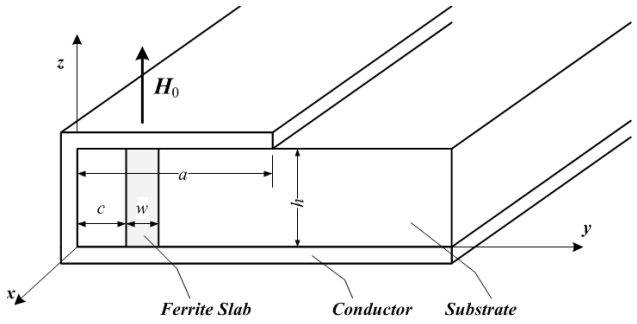

Figure 2. Configuration of the ferrite-load HMSIW.

In (2),

$$k_f^2 = (2\pi f)^2 \mu_e \varepsilon_f - \beta^2, \quad k_d^2 = (2\pi f)^2 \mu_d \varepsilon_d - \beta^2, \quad \mu_e = \left(\mu^2 - \kappa^2\right)/\mu$$

μ_d, ε_d are the relative permeability and permittivity of the dielectric substrate. μ_f, ε_f are the effective permeability and permittivity of the ferrite material, respectively. Here, the differential phase shift, φ, provided by an l length ferrite-loaded HMSIW can be calculated by

$$\varphi = \left(\beta^+ - \beta^-\right) l \tag{3}$$

In (3), β^+ and β^- stand for propagation constants in the forward direction (positive κ) and in the reverse direction (negative κ), respectively.

2.3. Ferrite-Load Half Mode Substrate Integrated Waveguide Phase Shifter

As shown in Figure 3, a non-reciprocal phase shifter can be realized based on the ferrite-loaded HMSIW after adding two microstrip-to-HMSIW transitions. The used substrate is 0.635 mm thick Rogers6010 substrate. Its permittivity and loss tangent are 10.2 and 0.0023, respectively. The actual HMSIW width is 4 mm, the distance between adjacent metallic vias 0.8 mm, and the diameter of vias 0.4 mm.

The magnetic bias field plays a key role in adjusting the ferrite effective relative permeability, and then control the differential phase shift, which is the difference between the forward and reverse phase shifts. As shown in Figure 4, a larger magnetic bias field leads to larger phase shift. As shown in Figure 5, the forward loss of the phase shifter is increased with the magnetic bias field, while the reverse loss keeps unchanged. Besides, the reverse loss is always less than the forward one. Here, Ansoft HFSS is used to obtain these analysis results. The YIG slab thickness is equal to the substrate thickness. The slab length, l, is 40 mm, the slab width, w, 1.4 mm, and the slab offset, c, 1.3 mm.

Next, let us discuss the influence of the ferrite slab dimensions. It is well known that a longer ferrite slab leads to larger differential phase shift and loss. Besides, a larger ferrite slab offset leads

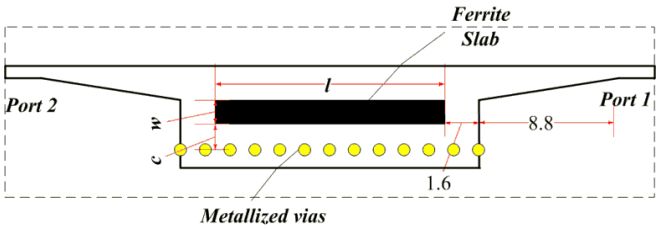

Figure 3. Configuration of the ferrite-load HMSIW phase shifter. (units: mm).

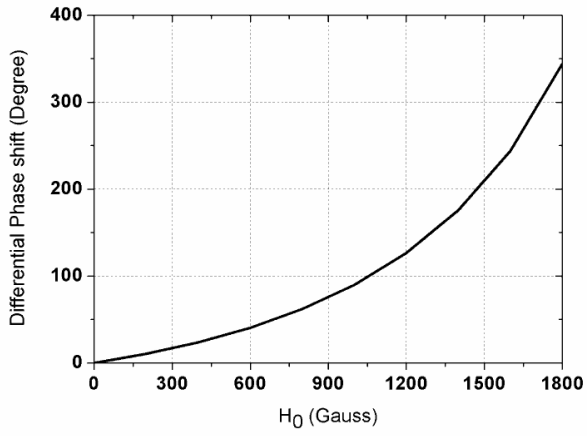

Figure 4. Magnetic bias fields versus differential phase shift values at 10 GHz.

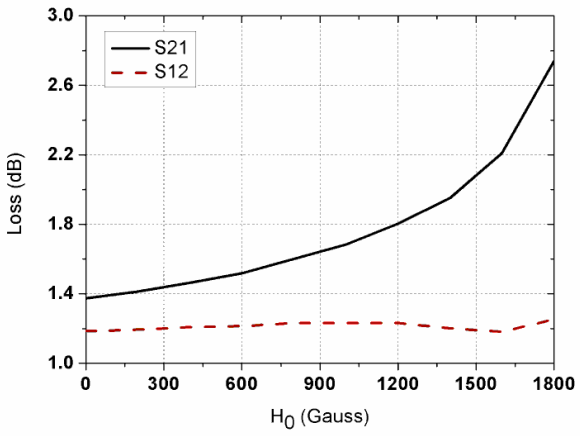

Figure 5. Magnetic bias fields versus insertion loss values at 10 GHz.

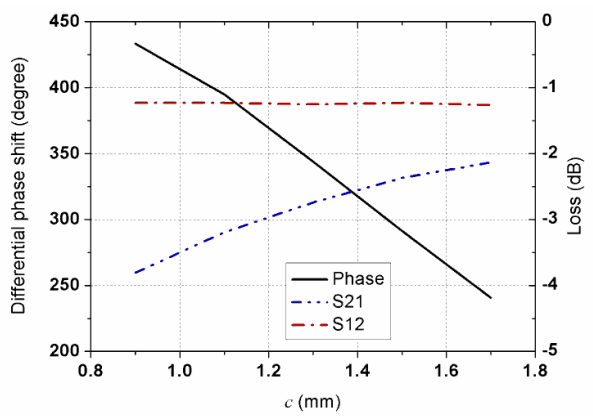

Figure 6. Phase shift and loss versus the ferrite slab offset at 10 GHz.

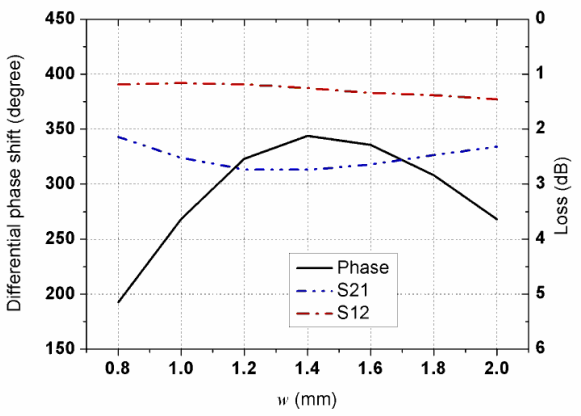

Figure 7. Phase shift and loss versus the ferrite slab width at 10 GHz.

to smaller forward phase shift but larger reverse phase shift as shown in Figure 6. The forward loss is decreased and the backward loss is increased with c. On the other hand, the ferrite slab width can also be used to adjust the phase shifting and loss characteristics of the ferrite-loaded HMSIW as shown in Figure 7. $w = 1.4$ mm leads to the largest phase shifting and loss. In these simulations, only the investigated parameter is changed, and others remain unchanged as described in the above paragraph. To achieve relatively small loss and good differential phase shift, $c = 1.2{\sim}1.4$ mm and $w = 1.2{\sim}1.6$ mm can be employed as the initial values.

3. EXPERIMENT

After full-wave optimization implemented by HFSS, the ferrite-loaded HMSIW phase shifter is fabricated as shown in Figure 8. Conductor tapes are used to cover the top and bottom of the ferrite slab. The required magnetic bias field is provided by an electromagnet. There exists a relationship between the internal field H_0 and the external field H_e

$$H_0 = H_e - NM_S \tag{4}$$

where N is the demagnetization factor as described in [21]. In general, the internal field H_0 is affected by the shape of the ferrite sample and its orientation with respect to the external field. The external magnetic bias field can be measured using a Tesla meter. Compared with the designed and measured magnetic bias field values, the demagnetization factor is about 0.65 in this design.

Simulated and measured results are presented in Figures 9–10 for magnetic biases of $H_0 = 0$ Gauss and $H_0 = 1800$ Gauss. For $H_0 = 0$ Gauss, the insertion loss is less than 2 dB from 9.6 to 10.2 GHz. The return loss is better than 15 dB over the same frequency range. For $H_0 = 1800$ Gauss, the insertion loss is lower than 3.2 dB from 9.7 to 11.0 GHz, which is 2.91 dB at the center frequency of 10 GHz. The loss due to magnetic loss increases. As is well known, the magnetic loss increases with external magnetic bias and reach maximum near the ferromagnetic resonance region. The return loss is better than 10 dB over the same frequency range. It is demonstrated that the increase of magnetic loss leads to higher attenuation. Figure 11 depicted the measured phase shift values with different magnetic bias fields.

Figure 8. Photograph of the fabricated ferrite-loaded HMSIW phase shifter.

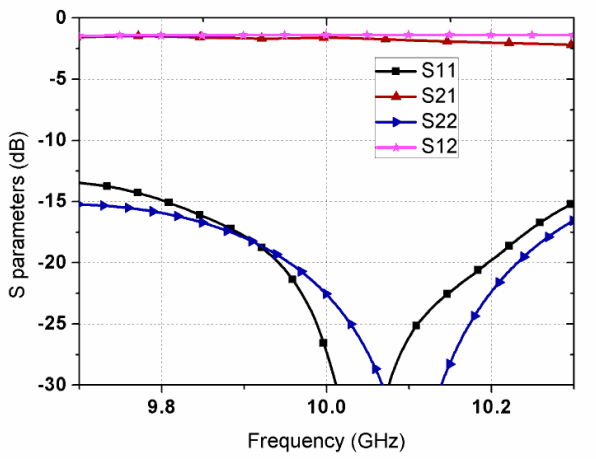

Figure 9. Measured S parameters of the ferrite-loaded HMSIW phase shifter for $H_0 = 0$ Gauss.

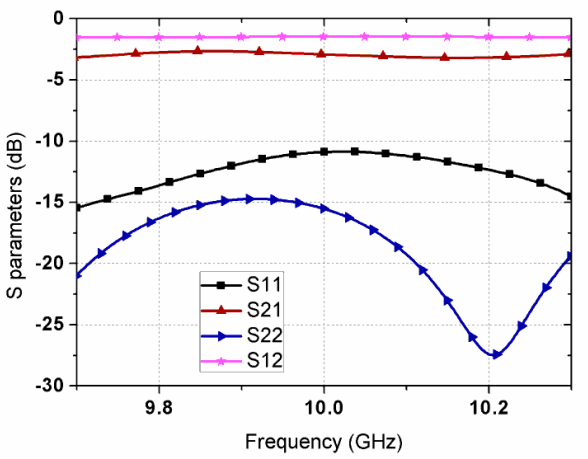

Figure 10. Measured S parameters of the ferrite-loaded HMSIW phase shifter for $H_0 = 1800$ Gauss.

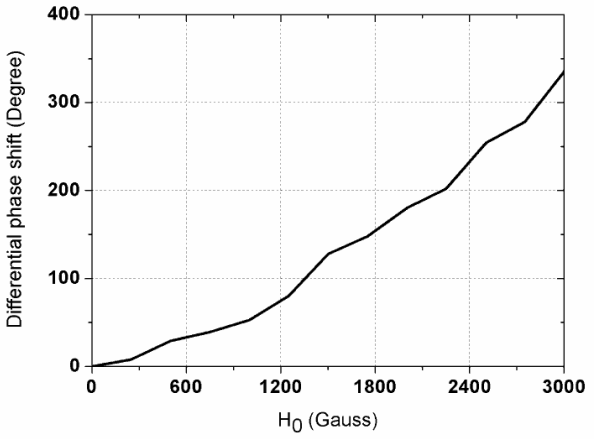

Figure 11. Measured differential phase shift values versus magnetic bias fields at 10 GHz.

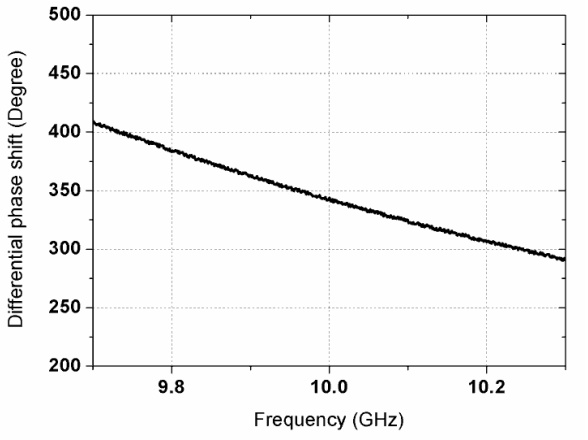

Figure 12. Measured differential phase shift of the ferrite-loaded HMSIW phase shifter versus frequency for $H_0 = 1800$ Gauss.

When H_0 is 1800 Gauss, the differential phase shift can reach to 337°. Figure 12 presents the measured differential phase shift of the ferrite-loaded HMSIW phase shifter versus frequency for $H_0 = 1800$ Gauss.

4. CONCLUSION

We design a ferrite-loaded HMSIW phase shifter at X-band. A rectangular slot is created in the HMSIW, where a full-height E-plane ferrite slab is inserted. Magnetic bias field is used to alter the effective permeability of the ferrite slab, which in turn changes the phase of the ferrite-loaded HMSIW. For the maximal magnetic bias field value $H_0 = 1800$ Gauss, the insertion loss is lower than 3.2 dB while the return loss is better than 10 dB from 9.7 to 11.0 GHz. Besides, the phase shift increases with the magnetic bias field to a maximum of 337°. It is an excellent candidate for microwave and millimeter-wave planar integrated applications.

ACKNOWLEDGMENT

This work is supported in part by the China Postdoctoral Science Foundation under grant 2013T60846 and 2012M511918.

REFERENCES

1. Uchimura, H., T. Takenoshita, and M. Fujii, "Development of 'a laminated waveguide'," *IEEE Trans. Microw. Theory Tech.*, Vol. 46, No. 12, 2438–2443, 1998.
2. Deslandes, D. and K. Wu, "Integrated microstrip and rectangular waveguide in planar form," *IEEE Microw. Wireless Compon. Lett.*, Vol. 11, No. 2, 68–70, 2001.
3. Cheng, Y. J., W. Hong, K. Wu, and Y. Fan, "Millimeter-wave substrate integrated waveguide long slot leaky-wave antennas and two-dimensional multibeam applications," *IEEE Trans. Antennas Propag.*, Vol. 59, No. 1, 40–47, 2011.
4. Cheng, Y. J., P. Chen, W. Hong, T. Djerafi, and K. Wu, "Substrate integrated waveguide beamforming networks and multibeam antenna arrays for low-cost satellite and mobile systems," *IEEE Antennas Propag. Mag.*, Vol. 53, No. 6, 18–30, 2011.
5. Liu, B., W. Hong, Y. Q. Wang, Q. H. Lai, and K. Wu, "Half mode substrate integrated waveguide (HMSIW) 3 dB coupler," *IEEE Microw. Wireless Compon. Lett.*, Vol. 17, 22–24, 2007.
6. Cheng, Y. J., W. Hong, and K. Wu, "Millimeter-wave half mode substrate integrated waveguide frequency scanning antenna with quadri-polarization," *IEEE Trans. Antennas Propag.*, Vol. 58, No. 6, 1848–1855, 2010.
7. Cheng, Y. J. and C. A. Zhang, "Miniaturized half mode substrate integrated waveguide cavity resonator and filter with good spurious suppression," *Journal of Electromagnetic Waves and Applications*, Vol. 27, No. 3, 396–404, 2013.
8. He, F. F., K. Wu, W. Hong, L. Han, and X. Chen, "A low phase-noise VCO using an electronically tunable substrate integrated waveguide resonator," *IEEE Trans. Microw. Theory Tech.*, Vol. 58, No. 12, 3452–3458, 2010.
9. Wu, L. S., X. L. Zhou, and W. Y. Yin, "A new type of periodically loaded half-mode substrate integrated waveguide and its applications," *IEEE Trans. Microw. Theory Tech.*, Vol. 58, No. 4, 882–893, 2010.
10. Sekar, V., M. Armendariz, and K. Entesari, "A 1.2–1.6-GHz substrate-integrated-waveguide RF MEMS tunable filter," *IEEE Trans. Microw. Theory Tech.*, Vol. 59, No. 4, 855–876, 2011.
11. Ding, Y. and K. Wu, "Varactor-tuned substrate integrated waveguide phase shifter," *International Microwave Symposium*, 1–4, Baltimore, US, Jul. 2011.
12. Cheng, Y. J., "Substrate integrated waveguide frequency-agile slot antenna and its multibeam application," *Progress In Electromagnetics Research*, Vol. 130, 153–168, 2012.
13. Xiang, Q. Y., Q. Y. Feng, X. G. Huang, and D. H. Jia, "Substrate integrated waveguide filters and mechanical/electrical reconfigurable half-mode substrate integrated waveguide filters," *Journal of Electromagnetic Waves and Applications*, Vol. 26, No. 13, 1756–1766, 2012.
14. Khalichi, B., S. Nikmehr, and A. Pourziad, "Reconfigurable SIW antenna based on RF-MEMS switches," *Progress In Electromagnetics Research*, Vol. 142, 189–205, 2013.
15. Sellal, K., L. Talbi, and M. Nedil, "Design and implementation of a controllable phase shifter using substrate integrated waveguide," *IET Microw. Antennas Propag.*, Vol. 6, No. 9, 1090–1094, 2012.
16. Adhikari, S., Y. J. Ban, and K. Wu, "Magnetically tunable ferrite loaded substrate integrated waveguide cavity resonator," *IEEE Microw. Wireless Compon. Lett.*, Vol. 21, 139–141, 2011.
17. Ghiotto, A., S. Adhikari, and K. Wu, "Ferrite-loaded substrate integrated waveguide switch," *IEEE Microw. Wireless Compon. Lett.*, Vol. 22, 120–122, 2012.
18. Adhikari, S., A. Ghiotto, and K. Wu, "Simultaneous electric and magnetic two-dimensionally tuned parameter-agile SIW devices," *IEEE Trans. Microw. Theory Tech.*, Vol. 61, No. 1, 423–435, 2013.
19. Tan, L. R., R. X. Wu, C. Y. Wang, and Y. Poo, "Magnetically tunable ferrite loaded SIW antenna," *IEEE Antennas Wirel. Propag. Lett.*, Vol. 12, 273–275, 2013.
20. Fesharaki, F., C. Akyel, and K. Wu, "Broadband substrate integrated waveguide edge-guided mode isolator," *Electronics Lett.*, Vol. 49, No. 4, 269–271, 2013.
21. Pozar, D. M., *Microwave Engineering,* 4th edition, Wiley, New York, 2011.